

ARTICLES

Search for time-reversal-symmetry violation in thallium fluoride using a jet source

D. Cho, K. Sangster, and E. A. Hinds

Physics Department, Yale University, New Haven, Connecticut 06520

(Received 20 February 1991)

We have looked for a violation of time-reversal symmetry (T) in the molecule thallium fluoride using a rotationally cold beam from a jet source. Our method was to search for a frequency shift of the thallium nuclear magnetic resonance when an external electric field of 29.5 kV/cm was reversed with respect to a magnetic quantization axis. The measured shift, $(1.4 \pm 2.4) \times 10^{-4}$ Hz, was interpreted as a null result and constitutes a tenfold improvement in sensitivity over the previous measurement. Accordingly, our measurement has reduced the upper limits on the proton and electron electric dipole moments and on other T-violating weak couplings that can be deduced from the frequency shift.

I. INTRODUCTION

The discovery of parity violation in 1957 [1,2] triggered a very rich period in theoretical physics which led eventually to a much deeper understanding of electroweak interactions. By contrast, the appearance of CP violation in K^0 decay [3] is still, 26 years later, an isolated phenomenon and the cause of CP violation remains a mystery. The violation of CP invariance is very closely related to that of another invariance, time reversal (T), and in this paper we describe our search for a T-violating permanent electric dipole moment (EDM) in the molecule TlF.

A. Electric dipole moment and T violation

In order for a nondegenerate system to possess a permanent EDM along one of its angular momenta, parity and time-reversal invariances must both be violated. We describe this as P&T violation. Accordingly, the EDM's of various atomic systems as well as that of the neutron have been measured in the hope of finding T violation that does not explicitly involve kaon decay [4]. Atoms or molecules are interesting places to look for T violation because they are composed of both leptons and hadrons and involve a wide range of fundamental interactions.

Atomic and molecular EDM measurements have all yielded null results so far and these have been used to put upper limits either on intrinsic EDM's of the constituent particles or on a variety of time-reversal odd interactions between them. The possibility that an atomic EDM could be induced by the intrinsic EDM of one of the constituent particles was first discussed in detail by Schiff [5]. To the extent that an atom or molecule is made of charged point particles bound together by the Coulomb force, there is no permanent EDM of the system, i.e., no linear Stark interaction in a weak electric field, even when the individual particles have an EDM. This is a consequence of the equilibrium condition that the total electrostatic force on each particle must vanish. Of course, this argument fails if the particles also interact magnetically, or if one of the particles has a finite size over which its charge and EDM are differently distribut-

ed. Schiff showed that through these mechanisms (we call them the magnetic effect and the volume effect, respectively) the EDM of a constituent particle would induce an EDM of the whole atomic system. The TlF molecule which we have studied includes relativistic (magnetically interacting) electrons and nuclei of finite size and therefore both of Schiff's mechanisms are operative [6-9]. Consequently, we are able to interpret our result as a measurement of the intrinsic electron and proton EDM's.

A different possibility is that the molecule may have a permanent EDM by virtue of P&T-violating interactions between its constituents [10,8] even in the absence of intrinsic EDM's. This allows us to deduce limits on P&T violation in both nucleon-nucleon and electron-nucleon interactions. Quite recently, Khriplovich [11] has noticed that our EDM measurement can also yield stringent limits on interactions that violate time-reversal symmetry while *conserving* parity. These various interpretations are discussed more fully in Sec. V.

The internal P&T-violating forces in an atomic system induce a permanent EDM by mixing states of the same spin and opposite parity. In this respect, a system having nearby states of opposite parity is more polarizable and therefore more sensitive to fundamental P&T violation. Sandars [6] pointed out that a polar molecule is such a system because a permanent dipole moment can be induced by the mixing of rotational levels, which are typically very much closer in energy than the levels of an atom. In addition, a heavy nucleus is desirable because it enhances both the magnetic and the volume effect. Following Sandars original suggestion, many attempts have been made to detect a permanent EDM of the TlF molecule [12-15]. This particular polar molecule is appealing because it is chemically stable, easily vaporized and detected, has simple structure and includes a heavy nucleus (Tl).

The result reported here, first published in a Letter [16], constitutes a substantial advance over previous experiments on TlF and contributes at a significant level to our knowledge of T violation in nature. The main reasons for this progress have been two technical developments. First, we devised and implemented a pure TlF supersonic jet source which produced an intense, rota-

tionally cold molecular beam and allowed a great improvement in the signal-to-noise ratio of our measurement. Second, we introduced a reversal into the experiment which increased our ability to distinguish spurious instrumental effects from the true EDM signal. These innovations jointly led to a tenfold improvement in our measurement of T violation in TIF.

B. Principle of the experiment

Stripped to the bare essentials, our experiment involved the spin-polarized TIF molecule, placed in an electric field E_C . Nuclear magnetic resonance (NMR) was performed on the Tl nucleus and we looked for a linear Stark effect by searching for a shift of the NMR frequency when E_C was reversed.

The interaction of the Tl nuclear spin $\frac{1}{2}\hbar\sigma$ with the rest of the molecule can be described by the effective Hamiltonian

$$H = -\mu_{\text{Tl}}\sigma \cdot \mathbf{B}_0 - dh\sigma \cdot \hat{\lambda}. \quad (1)$$

The first term is the usual (T-conserving) hyperfine interaction of the nuclear magnetic dipole moment $\mu_{\text{Tl}}\sigma$ with the internal magnetic field \mathbf{B}_0 of the molecule. On the other hand, the second term describes the P&T-violating electric dipole interaction that we are interested in. Here $\hat{\lambda}$ is a unit vector pointing from the Tl nucleus to the F nucleus, d is a measure of T violation in TIF, and h is Planck's constant. In free space, such an interaction would tip the internuclear axis, giving it a small projection along σ , and hence producing a small permanent EDM. We prefer, however, to detect this interaction by applying the strong field E_C , which substantially polarizes $\hat{\lambda}$, and to look for an energy of the form $\sigma \cdot E_C$. This energy appears as a shift of the NMR frequency when E_C is reversed.

A schematic view of the experiment is shown in Fig. 1.

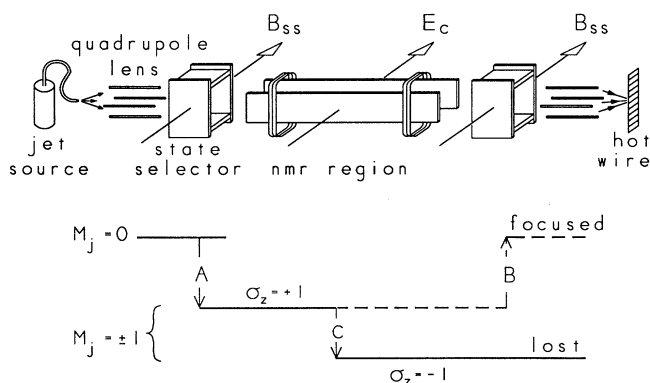


FIG. 1. Schematic view of the experiment. State selector transition A places focused $M_J=0$ molecules into a single magnetic sublevel of the $M_J=\pm 1$ manifold. Transition B is the inverse of A . The main resonance, labeled C , is the Tl nuclear spin flip.

A beam of molecules was produced by a supersonic jet source. The temperature of the molecules was sufficiently low that they were all in the electronic ground state and most of them were in the vibrational ground state ($^1\Sigma$, $v=0$). On the other hand, a large number of rotational and hyperfine states were occupied, although our measurement was performed using only one particular magnetic hyperfine sublevel of the first excited rotational state $J=1$.

Within $J=1$ there are 12 magnetic hyperfine sublevels corresponding to the three projections of $|J=1\rangle$ and the two projections of each spin- $\frac{1}{2}$ nucleus. In order to select a particular one of these magnetic sublevels, we used the combination of an electrostatic quadrupole lens together with a so-called state selector. First, the lens focused those molecules having ($J=1$, $M_J=0$) and deflected the $M_J=\pm 1$ molecules out of the beam. Next, the four nuclear spin states were resolved in the state selector by a 27 G magnetic field, and finally an oscillating electric field drove a transition (schematically shown as A in Fig. 1) from one of these states to one of the eight sublevels in the manifold ($J=1$, $M_J=\pm 1$). These were the molecules on which our measurement was made. The Tl nuclear spin transition (labeled C in Fig. 1) was induced in them using separated oscillating magnetic fields to produce a narrow Ramsey resonance line. Finally, a second combination of state selector (transition B) and electric quadrupole rendered the NMR transition observable: it focused the beam onto a hot wire detector when σ was unchanged, but defocused it when σ had been flipped.

II. APPARATUS

A. Overview

The molecular-beam machine was built specifically to perform this experiment [17]. The apparatus was 5.3 m long and consisted of three regions: a source chamber, a main beam line, and a detector chamber. The main beam line had T-shaped aluminum chambers at each end, which housed the electrostatic quadrupoles, and a central 3.0-m-long Pyrex tube contained the state selectors and NMR region. The source, detector, and aluminum T's were pumped by four oil diffusion pumps which maintained a background gas pressure below 1.0×10^{-7} Torr.

B. Source

The source (Fig. 2) consisted of a heated copper cylinder, containing hot liquid TIF, and a long nozzle through which the vapor escaped to form a beam. Two hundred grams of TIF lasted for a few months, after which the lid could be removed and a fresh charge loaded. A corrugated piece of copper sheet (boiling chip) was put inside the container together with the TIF in order to spread the heat evenly. Thermal insulation and mechanical support of the source were both accomplished by an alumina fiber blanket (Fiberfrax made by Carborundum) which was in turn held in a stainless-steel jacket. The nozzle was made from a 30 cm length of 1.5-mm-bore copper tube which we squeezed down to 0.5 mm at the

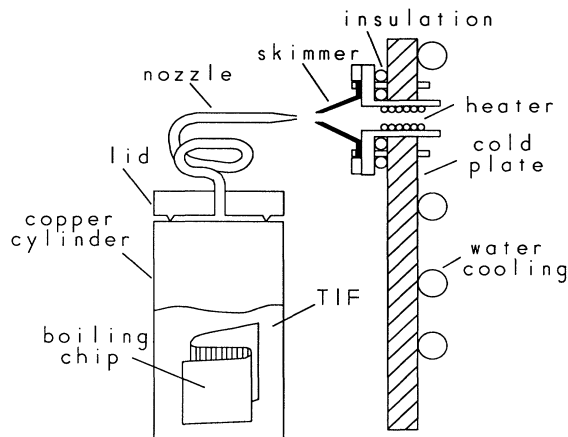


FIG. 2. Supersonic TlF source and skimmer. Use of the long heated nozzle reduces the dimer fraction. The skimmer was heated because TlF is solid at room temperature. The cold plate helped to keep the background pressure low.

exit. The container and nozzle were heated to 750 and 780 K, respectively, using commercial coaxial heater wire (Thermocoax).

Inside the source chamber, immediately downstream from the source hole, there was a heated conical skimmer mounted on a water-cooled plate. It had an aperture of 1.5 mm diam, which allowed the core of the jet to pass through. Under our operating conditions, however, the presence of the skimmer did not make a substantial difference to the quality of the beam. Most of the TlF molecules that hit the water-cooled plate were condensed there, maintaining a low background pressure in the source chamber.

In our first attempts to produce a supersonic beam, we used a nozzle that was only 2.5 cm long. This design produced a large increase in the total beam intensity but only a modest improvement in the strength of our resonance signal, indicating that the population of $J=1$ molecules was not greatly improved. We presumed that the beam was condensing into clusters and introduced the long heated nozzle in order to superheat the TlF vapor before allowing it to expand in the hope that this would inhibit the condensation. In addition the pressure drop along the tube should favor the decomposition of dimers and polymers. We found that this method works—both the total beam and the resonance signal were enhanced in comparison with our previous effusive source. However, as the temperature was increased further, the resonance signal increased more slowly than the full beam and our operating temperature of 750 K represents an optimum with respect to the signal-to-noise ratio of the experiment.

The operation of the source is characterized not only by the intensity of the beam but also by the translational, rotational, and vibrational temperatures. Since the translational temperature is a measure of the velocity dis-

tribution of the molecules, we were able to determine it using the fact that the focal length of our electrostatic quadrupole lenses was strongly velocity dependent. The result was 300 ± 50 K, as we discuss more fully in Sec. II D. The rotational temperature is indicated by the distribution of rotational states. We were able to use the state-selector resonance strength to determine the fractional $J=1$ population and hence to deduce the rotational temperature 350 ± 50 K. Finally, the vibrational temperature was obtained from the NMR spectrum. Molecules in the first few vibrational levels gave rise to a multiplet of lines for each nuclear spin transition. The relative heights of these lines revealed the population distribution among the vibrational levels and indicated a vibrational temperature of 400 ± 50 K.

C. Detector

A hot, oxygenated tungsten filament (work function ~ 6.4 eV) was used to detect TlF molecules by surface ionization. Hot wires made of commercial tungsten are generally contaminated with potassium, which provides a large background ion signal. In order to avoid this problem, we grew our own tungsten surfaces by decomposing tungsten hexacarbonyl, $W(CO)_6$, on a hot tantalum foil substrate [18]. The filament was then used at a dull orange temperature and was continuously oxygenated by a jet of O_2 directed at its front surface in order to obtain a high work function. The ion current produced by the hot wire was amplified by an electrometer whose output voltage controlled the frequency of a pulse generator. The pulse string was fed in turn to a scalar controlled by a small computer. A typical detector background was 7.5×10^7 ions/sec and the detection efficiency for TlF was estimated to be 90%. The active detector area was defined by a 2.5-mm-diam aperture in front of the filament.

D. Electrostatic quadrupoles

The electric quadrupoles, shown schematically in Fig. 1, were made from aluminum rods 60 cm long with a semicircular cross section of radius 1.75 cm. When assembled, the inscribed circle had a radius of 1.16 cm. The potentials on the rods were typically set to ± 9 kV so that the field strength inside the quadrupole increased linearly from zero at the center to ~ 15 kV/cm at the edge. When considering the deflection of the molecule in this electric field we can neglect the magnetic interactions and consider only the Stark energy, which is adequately described by the rigid rotor Hamiltonian [19],

$$W = hBJ^2 - \mu_E E_C \cos \theta, \quad (2)$$

where B is the rotational constant and μ_E is the electric dipole moment of TlF. Of course μ_E is not the P&T-violating EDM that we are searching for. It is *not* directed along any of the angular momenta, but rather it lies along the direction of the internuclear axis $\hat{\lambda}$ and hence is not T violating. For TlF, the constants are $B = 6.69$ GHz and $\mu_E/h = 2.13$ MHz/(V/cm). The Stark shifts of the $J=1$ manifold are plotted in Fig. 3.

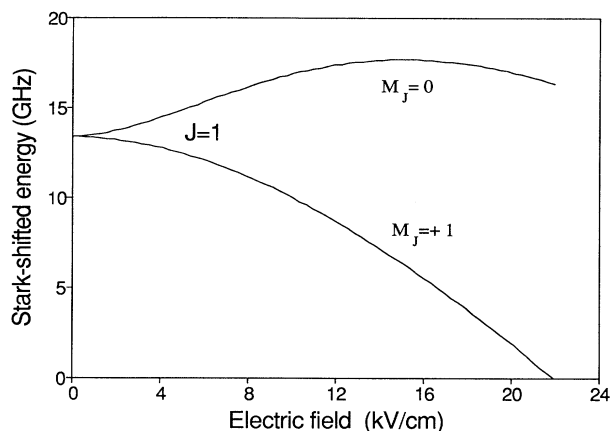


FIG. 3. Stark shift of TIF in $J=1$ manifold. When the electric field is less than 15 kV/cm, molecules in the $J=1$ manifold experience opposite Stark shifts. The low-field seeking state $M_J=0$ is focused in the quadrupole lens while $M_J=\pm 1$ is defocused.

As the beam passed through the electrostatic quadrupole, the ($J=1, M_J=0$) molecules were deflected toward the axis (focused) where their potential energy is lower, whereas the ($J=1, M_J=\pm 1$) beam was defocused. We used two identical electrostatic quadrupoles, one to collect the beam from the source and one to focus it onto the detector as shown in Fig. 1.

Just inside the entrance to the detector quadrupole we placed a movable beam stop of radius 1.2 mm to block the unwanted straight-through beam. This was made by spot welding a steel ball to two steel supporting wires at right angles to each other. Electrically the stop was grounded so that when the quadrupole was symmetrically charged, the supporting wires did not disturb the field.

To optimize the alignment, we grounded the quadrupoles and blocked as much of the beam as possible with the stop. Some scattered molecules were always detected, but the direct paths from source to detector were all blocked. The quadrupole potentials were then turned on and we observed an increase in the detector signal due to the focused beam. This was almost entirely composed of ($J=1, M_J=0$) molecules and was two orders of magnitude larger than the ($J=1, M_J=0$) population of the unobstructed straight-through beam. Thus the quadrupole lenses served a dual role, increasing the number of molecules available for NMR as well as helping to make the resonance observable.

The focused beam was measured as a function of the potential on the quadrupoles. At each voltage a different velocity is focused most efficiently, so the shape of this curve was closely related to the velocity distribution and hence to the translational temperature of the beam. When the quadrupole field was high, it began to focus slow $J=2$ as well as faster $J=1$ molecules; however, we were able to distinguish the $J=1$ component of the focused beam by measuring the number of molecules parti-

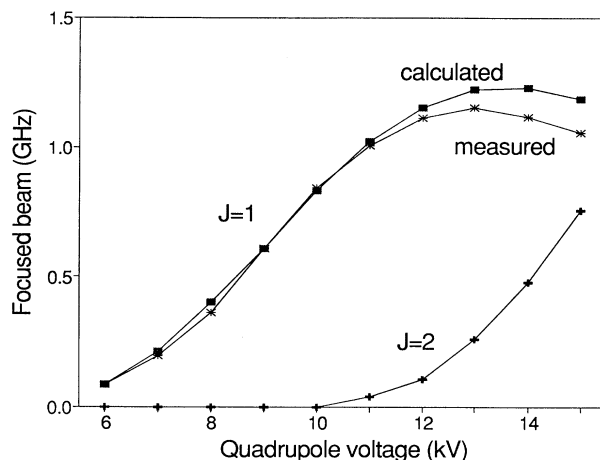


FIG. 4. Focused beam vs quadrupole voltage. Measurements of the total focused beam and of the state-selector resonance strengths yielded the $J=1$ and 2 profiles shown. Also shown is the calculated $J=1$ focused beam when we assume a translational temperature of 300 ± 50 K and a rotational temperature of 350 ± 50 K.

icipating in the state-selector resonances. The experimental result is shown in Fig. 4.

In the same figure we show the result of a computer model. For this we assumed that the molecules began in thermal equilibrium at the (known) nozzle temperature and then expanded at constant enthalpy, reaching a final state in which translational and rotational motions are in thermal equilibrium, at two (unknown) temperatures. The total output of TIF was determined experimentally

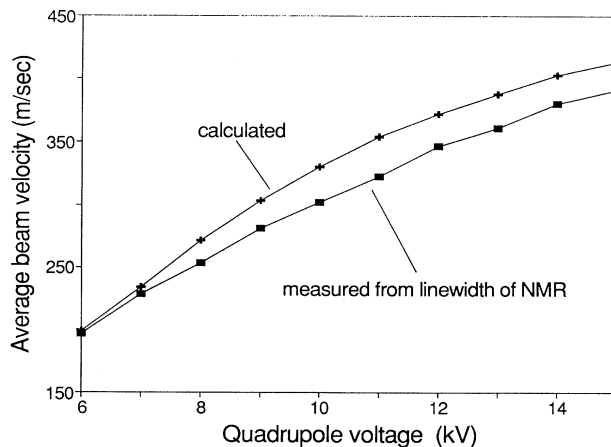


FIG. 5. Average beam velocity vs quadrupole voltage. We measured the average velocity of the $J=1$ focused beam as a function of quadrupole voltage by observing the linewidth of the NMR resonance. For comparison we show the calculated velocity assuming a translational beam temperature of 300 ± 50 K.

by measuring the total intensity of the beam without focusing, so the translational and rotational temperatures of the beam were the free parameters in the model. The shape of the curve in Fig. 4 depended primarily upon the former, while the latter controlled the scale. Excellent agreement was obtained between this model and our observations when the temperatures were taken to be 300 ± 50 and 350 ± 50 K, respectively.

The line width of the NMR resonance is proportional to the velocity of the beam. We used this fact to measure the average beam velocity versus quadrupole voltage as an independent check of the model. Figure 5 shows the experimental result together with the theoretical prediction based on the temperatures derived above. Considering the complexity of this problem, the agreement is very satisfactory.

We remark in passing that the focused $J = 2$ molecules gave rise to a troublesome background when we came to measure the EDM. Consequently, most of our data were taken at a focusing potential of ± 9 kV, where the focused beam was only half its peak value, but where virtually all of it was in the $J = 1$ state. The corresponding loss of statistical sensitivity was largely compensated by the narrower linewidth of the NMR resonance at lower quadrupole voltage.

E. State selectors

Within the electronic and vibrational ground state, the structure of the free TIF molecule is due both to its rotation and to the hyperfine interactions involving the two spin- $\frac{1}{2}$ nuclei. The Hamiltonian representing this structure can be written

$$H = H_{\text{rot}} + H_{S-R} + H_{S-S}, \quad (3)$$

where H_{rot} is the rotational energy, H_{S-R} couples the nuclear spins to the rotation, and H_{S-S} couples them to each other, both directly and via the electrons [20]. Detailed expressions for each of these terms together with numerical values for the coupling constants can be found in [14]. Of particular interest for our experiment are the twelve hyperfine sublevels within the $J = 1$ rotational state, which are conventionally labeled by A through L . Table I gives the eigenstates for those sublevels in the limit of high electric field—as they are in the NMR region and in the quadrupoles. We see that the four states A , B , C , and D are focused in the quadrupole field since they have $M_J = 0$.

Further selection of a particular hyperfine level was achieved by the state selector which induced a transition from one of these four focused states to one of the eight states that are deflected out of the beam by the quadrupole. This transition was driven by an oscillating electric field in the presence of a 27-G static magnetic field \mathbf{B}_{SS} and a 35-V/cm static electric field \mathbf{E}_{SS} . The purpose of \mathbf{B}_{SS} was to resolve the magnetic sublevels so that a single magnetic state could be selected. The static electric field \mathbf{E}_{SS} made it possible for the oscillating electric field to drive the transition: in the absence of \mathbf{E}_{SS} this $E1$ transition would be forbidden by the parity selection rule since

both states belong to the same $J = 1$ manifold. In our experiment we used the transition $A \rightarrow J$ at 300 kHz or $D \rightarrow K$ at 197 kHz to select either J or K , respectively, as the initial state for the NMR transition.

The construction of the state selectors is shown in Fig. 6. The electromagnet was built on a rectangular frame made of a high permeability low-hysteresis material (Advance Magnetics Ad-Mu80) in order to shield the ambient field and to ensure accurate reversal of the applied magnetic field. The electric field was formed by five pairs of aluminum plates separated by 2.4 cm. A ground strip along the top and bottom helped to keep the field uni-

TABLE I. Eigenvectors of $J = 1$ states of TIF in high electric field. Due to the Stark interaction, rotational angular momentum J is no longer a good quantum number and the label $J = 1$ is valid only in an asymptotic sense. M_1 and M_2 are the magnetic quantum numbers of the Tl and F nuclear spins, respectively.

Label	$ M_J, M_1, M_2\rangle$
A	$\left 0, -\frac{1}{2}, -\frac{1}{2}\right\rangle$
B	$\frac{1}{\sqrt{2}} \left 0, +\frac{1}{2}, -\frac{1}{2}\right\rangle - \frac{1}{\sqrt{2}} \left 0, -\frac{1}{2}, +\frac{1}{2}\right\rangle$
C	$\frac{1}{\sqrt{2}} \left 0, +\frac{1}{2}, -\frac{1}{2}\right\rangle + \frac{1}{\sqrt{2}} \left 0, -\frac{1}{2}, +\frac{1}{2}\right\rangle$
D	$\left 0, +\frac{1}{2}, +\frac{1}{2}\right\rangle$
E	$\left -1, -\frac{1}{2}, -\frac{1}{2}\right\rangle$
F	$\left +1, +\frac{1}{2}, -\frac{1}{2}\right\rangle$
G	$\left -1, -\frac{1}{2}, +\frac{1}{2}\right\rangle$
H	$\left +1, +\frac{1}{2}, +\frac{1}{2}\right\rangle$
I	$\frac{1}{\sqrt{2}} \left +1, -\frac{1}{2}, -\frac{1}{2}\right\rangle + \frac{1}{\sqrt{2}} \left -1, +\frac{1}{2}, +\frac{1}{2}\right\rangle$
J	$\left -1, +\frac{1}{2}, -\frac{1}{2}\right\rangle$
K	$\left +1, -\frac{1}{2}, +\frac{1}{2}\right\rangle$
L	$\frac{1}{\sqrt{2}} \left +1, -\frac{1}{2}, -\frac{1}{2}\right\rangle - \frac{1}{\sqrt{2}} \left -1, +\frac{1}{2}, +\frac{1}{2}\right\rangle$

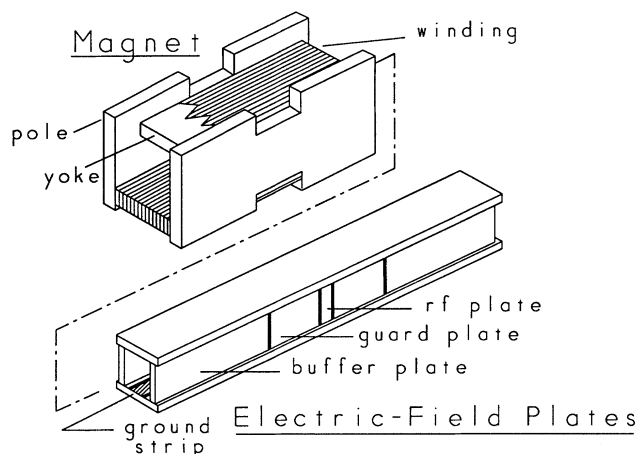


FIG. 6. Schematic view of a state selector consisting of two parts: magnet and electric-field plates. The magnet provided a uniform field of 27 G to resolve hyperfine levels. Electrostatic field of 35 V/cm was applied to both rf and guard plates, and 250 V/cm to the buffer plates. Oscillating electric field was applied to the rf plates to drive the state-selector resonances.

form across the height of the molecular beam. The rf field was produced only by the middle pair of plates, whereas the electrostatic potential difference was applied also to the guard plates on either side. This arrangement ensured that the static field E_{SS} was homogeneous even in the fringes of the rf field.

Since the quadrupoles and the NMR region employ fields of many kV/cm, the molecules must experience large and quite rapid changes of electric field at each end of the state selector. A number of level crossings occur in going between low and high field, and we noticed in particular that state J could easily make a Majorana (nonadiabatic) transition to state I in the fringe field of the magnet. In order to have some control over this region, we used the outer buffer plates shown in Fig. 6. These provided a uniform electric field of approximately 250 V/cm in the regions of magnetic fringe field and were largely successful in preventing unwanted transitions.

As a direct measure of state selector efficiency, the resonance strengths were compared with the number of focused molecules, one quarter of which could be expected to participate in either of the transitions. When the first state selector was turned on, we observed resonance strengths of 8.3×10^7 molecules/sec for transition $A \rightarrow J$ and 6.7×10^7 molecules/sec for transition $D \rightarrow K$, which seemed to imply efficiencies of 75% and 60%, respectively. The same result was found using the second state selector and when the two were used together to drive the sequence of transitions $A \rightarrow J \rightarrow A$ we confirmed that the $A \rightarrow J$ efficiency was indeed 75%. However, the sequence $D \rightarrow K \rightarrow D$ revealed that the $D \rightarrow K$ efficiency was in fact also 75% and that the number of focused molecules in state D was actually less than a quarter of the total. We suspect that the missing molecules were being lost between the quadrupoles and the state selectors, but no adjustment of the buffer plates was able to cure this prob-

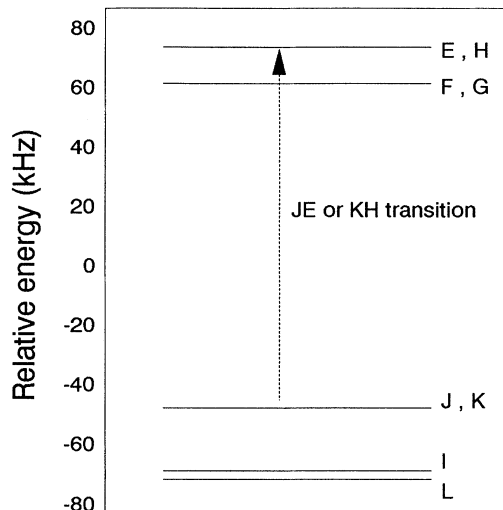


FIG. 7. Hyperfine sublevels of ($J=1, M_J=\pm 1$) in an electric field of 29.5 kV/cm. The zero of energy is arbitrary. The pairs of states (E, H), (F, G), and (J, K) are degenerate doublets in the absence of magnetic field. However, the $M_F=0$ states I and L are split as a result of the tensor interaction between the T1 and F nuclei. The transitions used in the experiment were $J \rightarrow E$ and $K \rightarrow H$.

lem. Both resonances had a linewidth of 16.4 kHz (full width at half maximum), which was due to the transit time through the rf field.

F. Nuclear magnetic resonance region

The eight sublevels of the manifold ($J=1, |M_J|=1$) in the high electric field E_C are shown in Fig. 7. The NMR transition, that we excited was either $J \rightarrow E$ or $K \rightarrow H$ depending upon the state chosen by the state selectors. Since (J, K) and (E, H) are both degenerate pairs, the two transitions were resonant at the same frequency $f_0 = 119.57$ kHz at $E_C = 29.5$ kV/cm.

The resonance was driven by a pair of separated oscillating magnetic fields of frequency f whose relative phase was switched under computer control between $\pm\pi/2$. The difference signal, plotted as a function of frequency, produced the antisymmetric Ramsey line shape [21] shown in Fig. 8. Near the center of the line this difference signal is well characterized by

$$S = I_0 \sin[2\pi T(f - f_0)], \quad (4)$$

where I_0 is the peak number of molecules per second in the resonance signal and T is the time of flight between the two separated oscillating fields. Each field was generated by a current of approximately 160 mA rms flowing in a 20-turn-coil of 21.6 cm diam. These coils were coaxial with the beam tube and were separated by 215 cm.

It is pleasing for us to compare the resonance strength observed using our jet source, $\sim 4 \times 10^7$ molecules/sec, with that obtained previously [17]. The strength of the transition has been increased by a factor of 50, even though the quadrupoles now work at half of their best

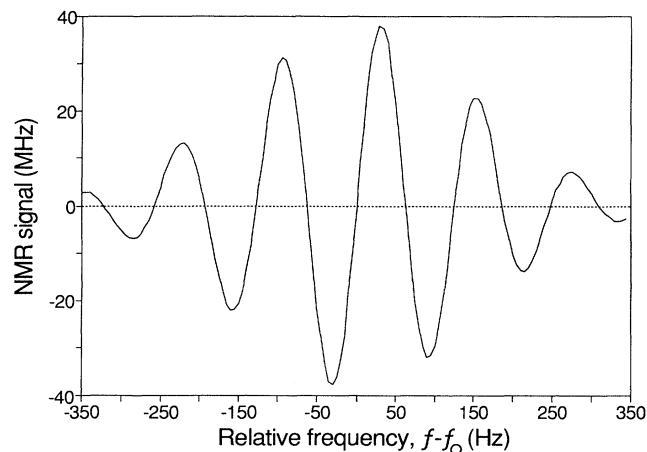


FIG. 8. Antisymmetric line shape of Tl NMR signal produced by the separated oscillating field method. We plot the difference in the signal strength as the relative phase between the separated oscillating fields is switched between $+\pi/2$ and $-\pi/2$. The curve crosses zero at the resonance frequency, $f_0 = 119.57$ kHz, and has a linewidth of 130 Hz. The slope of the line at the resonance determined the sensitivity of our measurement.

efficiency due to the reduced voltages (Sec. II D). Moreover, this large improvement in the signal strength was accompanied by an increase in the background of only 2.5 times (from detector and scattered beam). The sum of background and focused beam, the latter being no longer negligible, has increased by a factor of 4.

The resonance signal shown in Fig. 8, was produced by the main isotope ^{205}Tl (naturally 70.5% abundant) with the molecule in its vibrational ground state. However, this line was accompanied by several nearby smaller resonances due to the higher vibrational states and to the other isotope ^{203}Tl . The relative heights of these resonances allowed us to determine that the vibrational temperature of the beam was 400 ± 50 K. Consequently, we could estimate the fraction of state-selected molecules able to participate in the main resonance, and concluded that the NMR efficiency was as high as 97%. The efficiency could also be deduced by comparing the NMR signals produced by one coil and two coils. This method gave the same result. Of course, such a high transition probability was only possible because of the narrow velocity distribution of the state-selected supersonic beam.

The electric-field plates in the NMR region were 245 cm long, 7.6 cm wide, and 0.95 cm thick, and were spaced 2.0 cm apart. They were supported from the back by ceramic posts as shown in Fig. 9. The material used was aluminum because it is nonmagnetic and the surfaces were polished with a great care to achieve stability of the high electric field. When we reversed this field, it was important to keep the magnitude as constant as possible so as to avoid a Stark shift of the NMR frequency. For this purpose, we built a motor-driven rotary switch which was able, within 0.2 V, to reverse to the 59-kV potential difference applied between the plates. However, the total

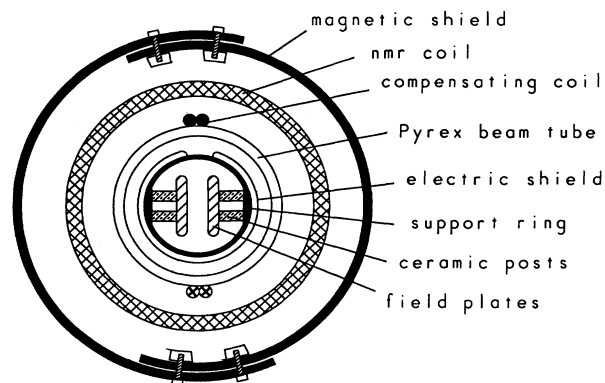


FIG. 9. Cross-sectional view of the NMR region. Inside the Pyrex tube we had the assembly of parallel electric-field plates to apply E_C , and slotted shields to reduce stray field from static charge on inner surface of the Pyrex. Outside were two coils that produced the rf magnetic fields, a magnetic shield, and compensating coils to null the residual ambient field.

electric field did not reverse so well at first because it was influenced by static charges that accumulated on the inside of the Pyrex beam tube. Later, we lined the glass tube with an electric shield made of grounded aluminum cylinders which satisfactorily suppressed the stray fields (Fig. 9). These cylinders had to be slotted along their length to avoid azimuthal currents being driven around them by the rf field.

In the NMR region the external magnetic field was supposed to be zero. We therefore enclosed the whole region within a highly permeable (Ad-Mu80) cylinder 30 cm in diameter. After this shield was installed and degaussed, the 120-mG ambient laboratory field along the direction of E_C was reduced to 0.5 mG. The residual field was further canceled by means of a compensating coil inside the magnetic shield which ran along the length of the Pyrex tube, as shown in Fig. 9. When we made our EDM measurements we found that this compensating coil was also useful for dealing with stray fields produced by the state-selector magnets (Sec. IV B 1).

III. MEASUREMENT

A. Modulations and reversals

In order to isolate the Tl NMR signal from the various detector backgrounds, we switched the relative phase of the separated oscillating fields between $\pm\pi/2$ as discussed in Sec. II F. We call this phase-switching P modulation.

At resonance, $f = f_0$, the line shape given in Eq. (4) shows that $\partial S/\partial f_0$ is maximum and $\partial S/\partial I_0$ is zero, making this an ideal place to look for a small shift of the resonance frequency. In practice, however, we changed the oscillator frequency between two values f_+ and f_- , symmetrically above and below the resonance by 1.25 Hz. This was called the F modulation. It allowed us to deter-

mine the slope of the resonance, which we needed in order to interpret changes of the observed signal strength as shifts in the resonance frequency. Furthermore, this offset from f_0 prevented the derivative $\partial S/\partial I_0$ from vanishing completely and allowed us to monitor changes of the resonance intensity I_0 as well.

Now we turn to the three main reversals employed in our experiment. The first of these, E modulation, involved a reversal of the sign of the electric field E_C . This reversed the polarization of the molecule $\langle \hat{\lambda} \rangle$ but did not affect any of the angular momenta and, in accordance with Eq. (1), produced a change of $-4d|\langle \sigma \cdot \hat{\lambda} \rangle|$ in the resonance frequency. We define the quantity S_{EDM} to be half of the total frequency shift,

$$S_{EDM} = -2d|\langle \sigma \cdot \hat{\lambda} \rangle|. \quad (5)$$

Note that electric-field reversal is similar to performing a parity transformation. In order to approximate this as closely as possible in our experiment, we reversed all the electric fields in the apparatus, i.e., state selector and quadrupole fields as well as E_C . Ideally one might also have hoped to reverse the beam velocity, but this was not done.

Our second main reversal, B modulation, changed the sign of the magnetic fields B_{SS} in the state selectors. Since the state-selector resonance populated a specific magnetic sublevel (either J or K) relative to the direction of B_{SS} , this modulation reversed the signs of all the chosen angular momenta relative to an axis fixed in the laboratory. In the language of Eq. (1), this corresponded to a reversal of the TI spin σ and of the internal magnetic field B_0 . Consequently, it produced the same frequency shift $2S_{EDM}$ as E modulation, but by an experimentally independent method. Note that this reversal of the angular momenta and magnetic fields was very similar to a time-reversal transformation although, again, we did not reverse the beam velocity.

The third primary modulation also allowed us to reverse the magnetization state of the molecule, but this time without changing the state-selector magnetic fields B_{SS} . This so-called M modulation was accomplished by changing the frequency of the rf fields in the state selectors so as to switch between the $A \rightarrow J$ and $D \rightarrow K$ transitions. As shown in Table I, states J and K are time-reversed versions of each other, which is the reason they form a degenerate doublet in the NMR region. This M reversal was an addition to our experimental method and one which proved to be very helpful in both studying and eliminating various systematic effects.

The collection of data involved computer-controlled execution of all these reversals—P, F, E, B, and M—in a predetermined sequence which devoted equal time to all 2^5 possible configurations. In addition, we employed some manual reversals so that a particular state of the external electronics could be made to correspond to a variety of states of the fields inside the beamline. Four types of manual reversal were employed; E, B, and M, corresponding to the modulations described above; and Q, which was an interchange of the positive and negative

voltages applied to the quadrupole rods. The manual reversals helped us to distinguish genuine physical effects from purely instrumental ones.

B. Computer control

Our control program, written in the language FORTH, organized the modulations in a sequence which sought to maximize the duty factor while minimizing the noise from systematic and random fluctuations. The general scheme is illustrated in Fig. 10. After any parameter was switched, it was necessary to gate out the signal for some time until the transient response of the beam was over. Naturally, the reversals with the shortest gate time were made most frequently in order to make the best use of our running time. These were the P, M, and F reversals, which only required 20 msec to cover the time of flight of the molecular beam. They were operated as a set of three nested loops and are shown in Fig. 10 under the heading PMF.LOOP. The innermost loop modulated the phase in the pattern $(+, -, -, +, -, +, +, -)$, while the M and F loops used the shorter sequence $(+, -, -, +)$. As Harrison, Player, and Sandars have discussed [22], these switching patterns are preferable to the more obvious $(+, -, +, -, \dots)$ because they are better able to distinguish the true signal from time-dependent drifts of the

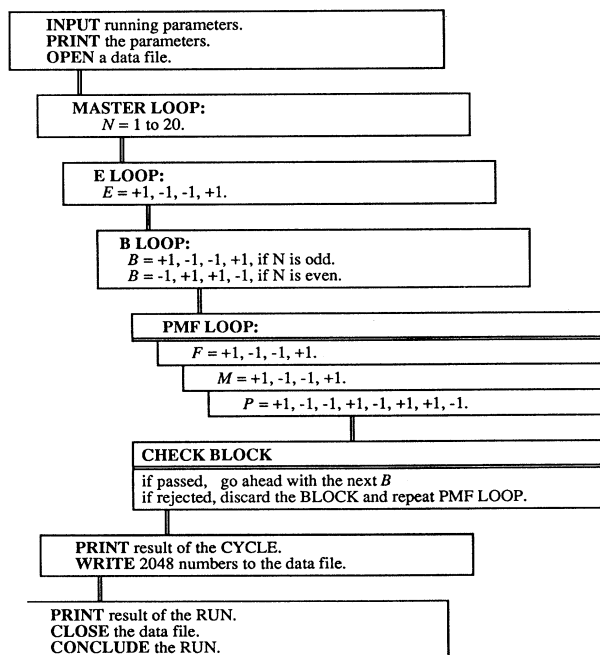


FIG. 10. Flow diagram of the data-taking program. Field reversals (E,B,M), phase (P), and frequency (F) modulations were performed in a nested sequence. Execution of one E LOOP completed a set of reversals and constituted one CYCLE of our EDM measurement. Twenty CYCLE'S constituted a MASTER LOOP and took about 80 min.

background. In addition, the signal does not need to be gated so often.

The magnetic field reversals required a 1.25-s gate time (to recover from the inductive transient) which placed them next in the nesting of loops—B.LOOP in Fig. 10. The longest gate was 20 sec, which we took to reverse the electric fields. During this time, the power supplies were first shut down and the potential difference across the plates was allowed to decay to a few kilovolts before the reversing switch was activated. The supplies were then turned on again and the plates recharged for 12.5 sec before the end of the gate period. Completion of one E.LOOP constituted a complete CYCLE. Note that the B.LOOP sequence was inverted every second CYCLE as a safeguard against transients associated with E modulation (see Sec. IV C 2).

In one execution of the PMF.LOOP the computer read the signal scaler 128 ($=8 \times 4 \times 4$) times, each reading being proportional to the number of ions detected over a 50-msec data acquisition period. At the end of each PMF.LOOP the numbers were grouped into two sets of 64 according to their M polarity and each group was checked for an excessive drift in the beam intensity. If any number deviated by more than 20 standard deviations from the mean of its group, the whole set was rejected and the PMF.LOOP was repeated. One rejection out of ten was typical, mainly due to pressure bursts in the beamline. After completing a CYCLE, the computer saved the 2048 ($=128 \times 4 \times 4$) scaler readings for future examination. A typical run, consisting of 20 CYCLES, lasted for 80 min of real time corresponding to a duty factor of 43%.

C. Data analysis

The state of the modulated fields was labeled by five variables as follows:

$$P = \begin{cases} +1 & \text{if the NMR phase equals } +\pi/2 \\ -1 & \text{if the NMR phase equals } -\pi/2 \end{cases}$$

$$F = \begin{cases} +1 & \text{if the frequency offset is } +1.25 \text{ Hz,} \\ -1 & \text{if the frequency offset is } -1.25 \text{ Hz,} \end{cases}$$

$$E = \{ +1 \text{ if E points west, } -1 \text{ if east,} \}$$

$$B = \{ +1 \text{ if B points west, } -1 \text{ if east,} \}$$

$$M = \begin{cases} +1 & \text{if the state selector drives the } A \rightarrow J \\ & \text{transition, } -1 \text{ if } D \rightarrow K \end{cases}$$

Among the many quantities that could be determined from a CYCLE of 2048 measurements, the one of primary interest was the P&T-violating frequency shift S_{EDM} defined by Eq. (5). Near the center of the NMR line, where the experiment was conducted, this shift was proportional to the NMR difference signal S [Eq. (4)]. Furthermore, it changed sign under a reversal of E, B, or M, but was independent of F. Thus the shift could be expressed as

$$S_{EDM} = k \sum_{i=1}^{2048} (P_i E_i B_i M_i) N_i, \quad (6)$$

where N_i is the scaler reading acquired during the i th data interval of the CYCLE and P_i , E_i , B_i , and M_i are the corresponding modulation variables. The conversion from scaler counts to frequency units was accomplished by the factor k , which we determined from the same data, for since the F modulation stepped the oscillator frequency between $f = f_0 \pm 1.25$ Hz, k was given by the relation

$$1.25 \text{ Hz} = k \sum_{i=1}^{2048} (P_i F_i) N_i. \quad (7)$$

Although our main interest was in determining S_{EDM} , it was important for our understanding of possible systematic effects to measure many other types of frequency shift as well. For example, the NMR frequency shift due to a change in the magnitude of E_C under E modulation is given by the quantity $S_E = k \sum_{i=1}^{2048} (P_i E_i) N_i$. Similarly, the part of S_E that changed sign when B_{SS} was reversed was given by $S_{EB} = k \sum_{i=1}^{2048} (P_i E_i B_i) N_i$. Table II summarizes the various frequency shifts that we defined by an obvious extension of this approach.

The field reversals were capable of changing the intensity of the NMR signal [I_0 in Eq. (4)] as well as the resonance frequency. For example, an imperfect reversal of B_{SS} could change the efficiency of the state selectors thereby altering the number of molecules selected for the NMR transition. We call this kind of effect an intensity shift and label it with Greek letters as opposed to the Latin font used for frequency shifts. Thus the intensity shift just described was given by the dimensionless asymmetry parameter

$$S_\beta = \frac{\sum_{i=1}^{2048} (P_i F_i B_i) N_i}{\sum_{i=1}^{2048} (P_i F_i) N_i}. \quad (8)$$

Other relevant intensity shifts are listed in Table II. The most important of these for our purposes is $S_{\epsilon\beta\mu}$, the NMR intensity change that is correlated with all three primary modulations E, B, and M.

Our identification of the signals S_{EDM} and $S_{\epsilon\beta\mu}$ as the frequency and intensity shifts, respectively, is valid only when the frequency offsets f_+ and f_- are placed symmetrically above and below the resonance frequency f_0 ; in

TABLE II. Names of the frequency and intensity shifts. The last frequency shift is called S_{EDM} , rather than S_{EBM} , to stress its physical meaning.

Field variable	Frequency shift	Intensity shift
E	S_E	S_ϵ
B	S_B	S_β
M	S_M	S_μ
EB	S_{EB}	$S_{\epsilon\beta}$
BM	S_{BM}	$S_{\beta\mu}$
ME	S_{ME}	$S_{\mu\epsilon}$
EBM	S_{EDM}	$S_{\epsilon\beta\mu}$

general these signals are combinations of the two physical effects. It is, however, very desirable to be able to measure the frequency and intensity shifts independently, so we servo-controlled the frequency of the NMR field to keep its average value as close as possible to f_0 . The error signal for this feedback loop was simply the average resonance strength $\sum_i P_i N_i$, which goes to zero when $(f_+ + f_-)/2 = f_0$. Of course, the corrections were added to the loop only after a full set of field reversals had been completed so that the servo could not induce any artificial frequency shifts.

IV. RESULT AND SYSTEMATICS

A. Result

Figure 11 shows the values of S_{EDM} measured in 28 runs carried out over a period of a week. The total running time was about 38 h, out of which 16 h were the net data-taking time. The mean of these results, taking into account a small systematic correction described in Sec. IV B 2, gives the final result of our experiment,

$$S_{\text{EDM}} = 0.14 \pm 0.24 \text{ mHz} \quad (9)$$

which we interpret as a null shift. The quoted error is entirely dominated by random uncertainties and is close to the noise expected from random counting statistics—0.19 mHz over our 16-h data-taking period. A careful study of numerous possible systematic effects led us to the conclusion that the systematic uncertainty was small. In the following sections we discuss some of the systematic effects that we encountered in our experiment and describe how we dealt with them.

B. Systematic effects of inexact reversals

1. Shifts under a single reversal

Table II lists the three frequency shifts involving a single field reversal. They are S_E , S_B , and S_M . We measured $S_E = -5.25 \pm 0.31$ mHz, which implied a change in the magnitude of E_C under E reversal of 0.13 V/cm.

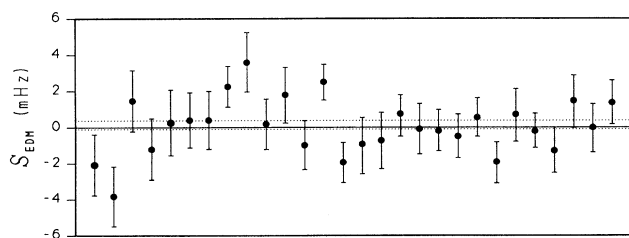


FIG. 11. Shifts S_{EDM} measured in 28 runs. Each data point is shown with an error bar of one standard deviation. The mean of these runs, 0.19 ± 0.24 mHz, lies between the dotted lines and we interpret it as a null shift. There was a small systematic correction to this number (Sec. IV B 2). However, it did not change our conclusion.

This was achieved only after building our own high-voltage switch and shielding the interaction region from the walls of the glass beam pipe (Sec. II F). We did not try to make any further improvement in the accuracy of electric-field reversal (although another order of magnitude reduction should be possible) because our EDM measurement used the additional reversals of B and M, to which the Stark shift was insensitive. However, this method of canceling the Stark asymmetry is only as exact as the reversals of B and M, and a fraction of S_E can appear in S_{EDM} if those reversals themselves are not exact. For this reason we also made sure that S_B and S_M were small.

The B and M modulations involved changes to the fields in the state selectors (magnet polarity and rf frequency). It was found that imperfections in these reversals did indeed cause a small modulation of the state-selector efficiency but could not, in any direct way, produce a shift of the NMR frequency. The most obvious cause of shifts S_B and S_M is the presence of a stray magnetic field in the NMR region. We distinguish two components of that field: the ambient field b_A and the fringe field from the state-selector magnets b_{SS} . Obviously the latter reverses under B modulation while the former does not. The total magnetic field at the site of the Tl nucleus is a combination of b_A , b_{SS} , and the internal (hyperfine) field B_0 , which depends upon the state of both B and M as summarized in Table III.

We see from Table III that S_B —the shift synchronous with B modulation and averaged over E and M modulation—is expected to be zero because it changes sign when M is reversed. Consequently, in order to detect the effect of the ambient field b_A , we had to measure the shift S_{BM} , which is equal to $2\mu_{\text{Tl}}b_A$. After installing and demagnetizing the shields, we found that S_{BM} was approximately 1 Hz, corresponding to b_A of order 500 μG , and this was further reduced to a few mHz by adjusting the current in the compensating coil (Sec. II F). The shift S_B we observed was -8.77 ± 0.25 mHz, indicating the existence of some M-independent shift synchronous with the B modulation. We do not know the origin of this effect, but suspect that it is related to the background signals discussed later in Sec. IV C 3.

The other part (b_{SS}) of the ambient field is given by S_M , which is equal to $2\mu_{\text{Tl}}b_{\text{SS}}$. This was initially some 5 Hz—by far the largest shift under a single reversal—indicating that b_{SS} was of order 2 mG. In an attempt to cancel this shift, we added to the compensating coil another current which reversed under B modulation and which reduced the shift by two orders of magnitude to approximately 40 mHz. Instead of making further, very fine adjustments of this current, we found it more satisfactory to null the S_M by introducing a compensating shift of the oscillator frequency when M was reversed. This was accomplished automatically by the lock loop that controlled the oscillator (Sec. III C), which maintained two separate feedback signals, one for $M = +1$ and one for $M = -1$.

We turn now to intensity shifts, which were primarily due to changes in the state-selector efficiencies. We

TABLE III. Various magnetic fields present in the NMR region and the associated frequency shifts. Unwanted external magnetic fields, b_A and b_{SS} , can combine with the internal field B_0 to produce shifts of type S_B and S_M .

	<i>AJE</i> ($M = +1$)		<i>DKH</i> ($M = -1$)	
	$B = +1$	$B = -1$	$B = +1$	$B = -1$
Internal field	B_0	$-B_0$	$-B_0$	B_0
Ambient field	b_A	b_A	b_A	b_A
State selector field	b_{SS}	$-b_{SS}$	b_{SS}	$-b_{SS}$
Total field strength	$B_0 + b_A + b_{SS}$	$B_0 - b_A + b_{SS}$	$B_0 - b_A - b_{SS}$	$B_0 + b_A - b_{SS}$
B.SHIFT	$2\mu_{T1}b_A$		$-2\mu_{T1}b_A$	
M.SHIFT			$2\mu_{T1}b_{SS}$	

found that S_ϵ and S_β were only a few parts per thousand. On the other hand, when both transitions $A \rightarrow J$ and $D \rightarrow K$ were optimized, the intensity shift S_μ was as large as 0.2 because of the difference between the A and D state populations that we discussed in Sec. II E. In order to compensate for this disparity, the rf power used for the $A \rightarrow J$ transition was reduced until equal numbers of state J and state K were produced. With this adjustment we obtained an average value of $S_\mu = (0.51 \pm 0.03)\%$ over our 28 runs.

Table IV presents a summary of the intensity and frequency shifts measured under the reversals E, B, and EB. The results for $M = +1$ and $M = -1$ are listed separately in the first two columns so that our measured values of all the shifts listed in Table II can be deduced. Specifically, column 3 shows the averages unweighted by M, namely, S_E , S_B , and S_{EB} , while column 4 gives the M-weighted averages, S_{EM} , S_{BM} , and S_{EDM} . The measured value of S_{EDM} , 0.19 ± 0.24 mHz, required a small systematic correction which we now discuss.

2. Coupling of frequency and intensity shifts

The combination of shifts S_E and S_β , or S_B and S_ϵ , produces a false shift S_{EB}

$$\Delta S_{EB} = S_\beta S_E + S_\epsilon S_B. \quad (10)$$

This shift is false because it appears even though the frequency shifts S_E and S_B are completely uncorrelated. In our experiment, this false shift was different for the two states $M = \pm 1$ and therefore generated a false EDM shift S_{EDM} of 0.05 mHz. Consequently, we subtracted 0.05 mHz from the total S_{EDM} to find the desired final shift. This was the only correction we had to make to S_{EDM} and since the measurement uncertainty is five times larger than the correction, it did not affect the conclusion drawn from our measurement.

3. Coupling of E and B fields

Suppose that the B modulation were accompanied by a small unintentional change $2\delta E_C$ of the electric field E_C in the NMR region. Then the magnitude of E_C would depend upon the relative sign of E and B, and through the Stark shift of the NMR line ($\delta f / \delta E_C = -41$ mHz/(V/cm) at 29.5 kV/cm) this would generate a frequency shift of the type S_{EB} . However, we could distinguish this from a genuine EDM effect because it would be insensitive to the sign of the M modulation and should average to zero when we average over M.

TABLE IV. Results averaged over the 28 runs. The first two columns show the shifts separated according to the M variable. In the third column they are combined to give the total shift averaged over M, and in the fourth column they are weighted by M.

	<i>AJE</i> ($M = +1$)	<i>DKH</i> ($M = -1$)	$(AJE + DKH)/2$	$(AJE - DKH)/2$
	Frequency shifts (mHz)			
E	-5.12 ± 0.40	-4.94 ± 0.41	-5.25 ± 0.31	0.13 ± 0.25
B	-11.66 ± 0.39	-6.19 ± 0.38	-8.77 ± 0.30	-2.65 ± 0.25
EB	-4.12 ± 0.35	-4.20 ± 0.34	-4.19 ± 0.25	0.19 ± 0.24
	Intensity shifts (%)			
ϵ	-0.62 ± 0.03	0.58 ± 0.03	0.00 ± 0.02	-0.60 ± 0.02
β	-0.27 ± 0.03	-0.16 ± 0.03	-0.22 ± 0.02	-0.05 ± 0.02
$\epsilon\beta$	0.01 ± 0.03	0.02 ± 0.03	0.02 ± 0.02	-0.01 ± 0.02

We found experimental evidence for just such an effect in our apparatus when the S_{EB} measurements were separated into $M=+1$ ($A \rightarrow J \rightarrow E$) and $M=-1$ ($D \rightarrow K \rightarrow H$) components:

$$S_{EB}(AJE) = -4.12 \pm 0.35 \text{ mHz}, \quad (11a)$$

$$S_{EB}(DKH) = -4.20 \pm 0.34 \text{ mHz}. \quad (11b)$$

The average value of -4.16 ± 0.24 mHz might be interpreted in terms of a changing electric field of $\delta E_C = 0.1$ V/cm as we have suggested above. However, we have not been able to find any mechanism to produce such a large change in the field and we think it is more likely that these apparent frequency shifts are an artifact associated with the background signals discussed below in Sec. IV C 3. We note that the M reversal was essential for distinguishing between this and a true EDM effect.

We turn now to the converse situation where the reversal of electric fields generates a change $2\delta B$ in magnetic field in the NMR region. The corresponding Zeeman shift of the NMR frequency appears as a shift S_{EB} that reverses with M, i.e., as an S_{EDM} . This is obviously a dangerous effect which our M reversal does not suppress and we have therefore taken some care to avoid it. We distinguish two contributions to δB . The first, δB_1 , is produced by the apparatus that reverses E (relays, electronic circuits, etc.), whereas the second, δB_2 , is caused by E itself. We were able to discriminate against effects due to δB_1 by a simple manual interchange of the electrical connections to the field plates, which changed the sign of E without affecting the switching apparatus. Any false EDM induced by δB_1 would change sign under such a reversal. Our measurements showed that there was no δB_1 effect at the level of precision achieved, but in any case we averaged over equal amounts of data taken with and without manual E reversal.

A false S_{EDM} caused by δB_2 is, by contrast, unchanged under manual reversal. Our only defense against this type of systematic error was to ensure that no significant current was drawn by the field plates. In our apparatus the current delivered to the high-voltage plates was always less than 2 nA at the operating voltage. We might imagine the worst possible circumstance, in which this current flows in a loop around the edge of each field plate, producing a magnetic field δB_2 of order 10^{-11} G. The false S_{EDM} that would result is entirely negligible, being five orders of magnitude smaller than the uncertainty in our measurement. In the absence of any significant current associated with E_C , we do not believe that δB_2 can be significant.

Even without leakage currents, there is still a motional magnetic field in the rest frame of the molecules. Indeed, this has been one of the most well known and troublesome systematic effects in beam resonance EDM experiments [23–26]. The high electric field E_C of the resonance region gives rise to a magnetic field $\mathbf{B}' \approx \mathbf{E}_C \times \mathbf{v}/c^2$ (SI units) in the molecular rest frame. If the angle θ between the applied electric and magnetic fields is not zero, this motional field adds an E-polarity-dependent modulation $b_M \sin\theta$ to the magnitude of the total B field: it

behaves exactly like a δB_2 . In our experiment, however, the magnetic field is not applied externally. On the contrary, the electric field provides the only symmetry axis for the system and therefore the internal magnetic \mathbf{B}_0 is precisely parallel to it. This is one of the important advantages of our working on a polar molecule.

C. Other systematics

1. Two-coil Millman effect

When the two separated NMR coils are misaligned, the geometric angle between the first and second fields can introduce a phase angle between the two rotating waves. This is essentially the Millman effect [27]. The phase difference leads to a frequency shift which changes sign under B and M reversals, contributing to the total value of the shift S_{BM} . Thus the S_{BM} that we have already discussed in the context of the ambient magnetic field (Sec. IV B 1) was actually due to a combination of the nonreversing ambient field and the Millman effect,

$$S_{BM} = \frac{2\mu_{T1}b_A}{h} + \frac{\theta}{2\pi T}, \quad (12)$$

where θ is the misalignment angle in the x-y plane and T is the time of flight between the two fields. We made use of the velocity-selective nature of the quadrupoles to obtain a plot of S_{BM} versus the linewidth ($1/T$) shown in Fig. 12. This allowed us to separate the two different parts of the shift and to determine that the Millman shift was approximately 140 mHz, corresponding to a misalignment angle $\theta = 6 \times 10^{-3}$ rad.

2. Transient effects

In order to study transient behavior of the NMR signals under E modulation, we compared values of S_E as

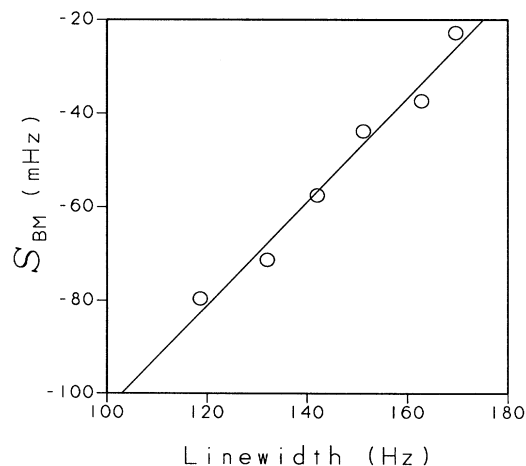


FIG. 12. Plot of the shift S_{BM} vs linewidth. The slope of this line allowed us to determine the Millman shift produced by a misalignment angle between the separated oscillating fields.

deduced from the first and second halves of the switching pattern (+, -, -, +):

$$\Delta E = S_E(+, -) - S_E(-, +), \quad (13)$$

which is sensitive only to the transient part of the signal and not to S_E itself. We found that ΔE was as large as 200 mHz even with a long gate time, 12.5 sec, after the high-voltage turn-on. This implied that at the end of the gating period E_C was still smaller than its final value by a few parts in 10^5 —probably because of a long settling time in the high-voltage supplies. Although it was not ideal to have such a transient shift, the additional B and M reversals were able to distinguish it from a true S_{EDM} . Similar tests to look for transient effects under B and M reversals revealed no effect.

3. Background signals

The state selector was carefully designed to make the desired $A \rightarrow J$ and $D \rightarrow K$ transitions with high efficiency and not to induce any other transitions. Nevertheless, we found that even when the rf fields in the state selectors were turned off, we could still observe small NMR signals in the vicinity of the $J \rightarrow E$ and $K \rightarrow H$ resonances. We measured the intensity of these lines as a function of the quadrupole voltages and concluded that they originated from the higher, most probably $J=2$, rotational states. In order to minimize the effect of this background in the experiment, we ran with the quadrupoles at a somewhat reduced voltage (Sec. II D). Further study of the background resonances revealed that they had the same Zeeman shift as the $J \rightarrow E$ (or $K \rightarrow H$) transition, but opposite Stark shift above 20 kV/cm. We used the latter property to separate them from the $J \rightarrow E$ and $K \rightarrow H$ transitions and this, in part, dictated our choice of $E_C=29.5$ kV/cm. With these adjustments we were able to reduce the background resonance strength to less than 5×10^{-3} of the main resonance lines. If these adjustments are not properly made, systematic variations of the background can make significant contributions to S_B , S_E , and S_{EB} . The background is, however, independent of the state selector rf field and therefore generates the same false shifts regardless of the M reversals. Consequently, even a large background did not produce a false S_{EDM} . With the background reduced as we have described, these anomalous shifts were also minimized; however, in the final data we still find the same type of M-independent shifts S_B and S_{EB} and we suspect that the residual background effects are responsible.

V. INTERPRETATION

TIF was originally proposed as a system for measuring an intrinsic proton EDM [6] because the Tl nucleus has one unpaired proton in the shell model. Obviously, that is not the only possibility for T violation in the complicated structure of the molecule. In this section we use our result to place limits on the various hypothetical T-violating mechanisms that might be present in TIF.

A. P&T-violating coupling constant

The phenomenological constant d that characterizes the strength of the P&T-violating coupling between the

TABLE V. Experimental limits on the P&T-violating coupling constant d in TIF.

Experiment	d (mHz)
Ref. [12]	-33 ±46
Ref. [13]	11 ±42
Ref. [14]	-8 ±12
Ref. [15]	2.4 ± 2.3
This work	-0.13 ± 0.22

Tl nuclear spin and the internuclear axis was defined in Eq. (1). It is related to our measured value of S_{EDM} and to $|\langle \sigma \cdot \hat{\lambda} \rangle|$ as shown in Eq. (5). In the strong applied electric field E_C , the hyperfine coupling between σ and J is overwhelmed by the Stark interaction with the result that $|\langle \sigma \cdot \hat{\lambda} \rangle|$ is approximately equal to $|\cos\theta|$, the projection of $\hat{\lambda}$ onto the electric-field direction. When the Stark-shifted energy is equated to $hBJ(J+1) - \mu_E E_C \cos\theta$, we find that for the electric field of 29.5 kV/cm used in our experiment, $\langle \cos\theta \rangle = 0.542$. Hence our experimental result [Eq. (9)] gives

$$d = -0.13 \pm 0.22 \text{ mHz} . \quad (14)$$

Table V summarizes the results of this and all previous experiments on TIF in terms of the same parameter d .

B. Molecular EDM

In the absence of any external fields, the P&T-violating internal interaction $H_{P\&T} = -dh\sigma \cdot \hat{\lambda}$ induces a permanent electric dipole moment d_{TIF} directed along the total angular momentum \mathbf{F} ,

$$\mathbf{d}_{TIF} = \sum_i \frac{\langle \psi_0 | \mathbf{D} | \phi_i \rangle \langle \phi_i | H_{P\&T} | \psi_0 \rangle}{E_0 - E_i} + \text{H.c.}, \quad (15)$$

where the electric dipole moment operator \mathbf{D} can be written as $\mu_E \hat{\lambda}$, $E_0 - E_i$ is the usual energy denominator, and H.c. denotes the Hermitian conjugate. For a particular value of d , the magnitude of d_{TIF} depends upon the hyperfine state of the molecule. In the $J=1$ states having total angular momentum $F=2$, we find that $d_{TIF} = d\mu_E / (10B)$ and therefore

$$d_{TIF} = (-1.7 \pm 2.9) \times 10^{-23} e \text{ cm} . \quad (16)$$

Of course, this EDM is the T-violating one along the total angular momentum, not the normal one along the internuclear axis. We note that the experimental uncertainty here is 2000 times larger than the uncertainty in the EDM of mercury [28], the smallest achieved in any system. The main reason for this disparity is that our resonance linewidth is due to the 10-ms transit time of the beam through the NMR region, whereas the coherence time of the mercury experiment was many minutes. On the other hand, our molecule is typically 2000 times more sensitive than mercury to the presence of T-violating fundamental interactions with the result that the two experiments are ultimately of comparable sensitivity.

C. Proton EDM

It is of interest to interpret our result in terms of the proton EDM because this experiment provides the smallest limit on it. If the proton has an intrinsic EDM d_p along its spin, the electric dipole interaction of the Tl nucleus is

$$H_{\text{P\&T(vol)}} = -d_p \sum_n \sigma_n \cdot \mathbf{E}(\mathbf{r}_n), \quad (17)$$

where $\mathbf{E}(\mathbf{r}_n)$ is electric field at the location \mathbf{r}_n of the n th proton. Under the constraint of the electrostatic equilibrium $\sum_n e\mathbf{E}(\mathbf{r}_n) = 0$, this interaction Hamiltonian can be rewritten [7] in our standard form $H_{\text{P\&T(vol)}} = -hd_{\text{vol}}\sigma \cdot \hat{\lambda}$, with

$$d_{\text{vol}} = d_p e \mathcal{D} X, \quad (18)$$

where e is the proton charge, \mathcal{D} is the difference between the mean-squared radii of the charge and dipole distributions in the nucleus, and $X\hat{\lambda}$ is $2\pi/3$ times the gradient of the electron probability density at the site of the Tl nucleus. In the above analysis the molecule is sensitive to d_p because the Tl nucleus has a finite volume over which the distributions of charge and dipole moment can differ—the volume effect [5]. Taking the values $X = 2128$ a.u. and $\mathcal{D} = 2.9 \text{ fm}^2$ recommended by Coveney and Sandars [8], one finds that the P&T-violating coupling constant d_{vol} induced in this way by a proton EDM is

$$\frac{d_{\text{vol}}}{d_p} = 2.75 \times 10^{18} \frac{\text{Hz}}{e \text{ cm}}. \quad (19)$$

The proton EDM also contributes to the total P&T-violating interaction through magnetic interactions. This also has the generic form $H_{\text{P\&T(mag)}} = -hd_{\text{mag}}\sigma \cdot \hat{\lambda}$, [5,13]. The value of this contribution is [29,30]

$$\frac{d_{\text{mag}}}{d_p} = 7.73 \times 10^{17} \frac{\text{Hz}}{e \text{ cm}}. \quad (20)$$

Taking both results together we find [8]

$$\frac{d_{d_p}}{d_p} = \frac{d_{\text{vol}} + d_{\text{mag}}}{d_p} = 3.52 \times 10^{18} \frac{\text{Hz}}{e \text{ cm}}. \quad (21)$$

Thus our experimental result [Eq. (14)] leads to a limit on the EDM of the proton:

$$d_p = (-3.7 \pm 6.3) \times 10^{-23} e \text{ cm}. \quad (22)$$

D. Nuclear EDM

Even if the proton and neutron themselves possess no permanent EDM, the Tl nucleus as a whole may still do so as a result of its structure. The interaction energy of the nucleus in the electrostatic potential $V(\mathbf{r})$ produced by the electrons is

$$W_{\text{Tl}} = \sum_n eV(\mathbf{r}_n), \quad (23)$$

where \mathbf{r}_n is the location of the n th proton as in Eq. (17). Once again, after invoking the electrostatic equilibrium condition, the effective P- and T-violating Hamiltonian

from this interaction can be written in our standard form [8,31]. The result is

$$H_{\text{P\&T}(Q)} = 6XQ\sigma \cdot \hat{\lambda} = -hd_Q\sigma \cdot \hat{\lambda}, \quad (24)$$

where Q , is the magnitude of the Schiff moment, defined by

$$Q = \frac{e}{6} \left[\frac{3}{5} \sum_n r_n^2 \mathbf{r}_n - \frac{1}{Z} \sum_n r_n^2 \sum_{n'} \mathbf{r}_{n'} \right]. \quad (25)$$

Since the expectation value of $Q(\text{Tl})$ must lie along the nuclear symmetry axis, we write Q as $Q\sigma$. Once again we take the value $X = 2128$ a.u., as calculated by Coveney and Sandars [8], to obtain the ratio

$$\frac{d_Q}{Q} = -5.67 \times 10^5 \frac{\text{Hz}}{e \text{ fm}^3}. \quad (26)$$

When combined with our experimental result this leads to a limit on the Schiff moment of the Tl nucleus:

$$Q_{\text{Tl}} = (2.3 \pm 3.9) \times 10^{-10} e \text{ fm}^3. \quad (27)$$

E. Electron EDM

The existence of an intrinsic electron EDM d_e will give rise to the P&T-odd Hamiltonian [32],

$$H_{\text{P\&T}(d_e)} = -d_e \beta (\sigma \cdot \mathbf{E} + i\alpha \cdot \mathbf{B}), \quad (28)$$

where α and β are the Dirac matrices. Flambaum and Khriplovich [9] have shown that when d_e is not zero, this interaction provides a P&T-violating coupling between the electrons and the nuclear spin of an atomic system. Obviously, such a coupling exists through the second term when \mathbf{B} is the field due to the nuclear magnetic moment. In addition, however, when the hyperfine interaction is included, the first term also becomes dependent on the nuclear spin and this makes an important contribution to the total interaction. We note that the Hamiltonian in its nonrelativistic limit is proportional to the total spin of electrons and therefore vanishes in the TIF molecule which has closed electron shells. However, the electrons in the vicinity of the Tl nucleus are highly relativistic and in fact d_e can induce an effective P&T-odd Hamiltonian $H_{\text{P\&T}(d_e)} = -hd_{e_e}\sigma \cdot \hat{\lambda}$. Following the calculations by Flambaum and Khriplovich [9], who considered the third-order perturbation that included the hyperfine interaction, we obtain the effective P&T-violating coupling constant for TIF

$$\frac{d_{d_e}}{d_e} = 6.24 \times 10^{20} \frac{\text{Hz}}{e \text{ cm}}. \quad (29)$$

When taken together with our experimental result this leads to a limit on the EDM of the electron:

$$d_e = (-2.1 \pm 3.5) \times 10^{-25} e \text{ cm}. \quad (30)$$

F. P&T-odd weak couplings

So far we have considered T violation in the molecule to be confined either to the nucleus or to the electrons.

Another possibility is that it may arise from P&T-odd weak couplings between the electrons and nucleons. Among the various Lorentz-invariant combinations of bilinear covariants of Dirac spinors it can be shown [33] that the scalar-pseudoscalar and tensor-pseudotensor interactions are odd under P and T. The scalar-pseudoscalar couplings, in the form of a contact interaction, are given as either

$$\langle H_{\text{P\&T}}^{(1)}(C_S^{(1)}) \rangle = iC_S^{(1)} \frac{G_F}{\sqrt{2}} (\bar{\psi}_n \psi_n) (\bar{\psi}_e \gamma^5 \psi_e) \quad (31a)$$

or

$$\langle H_{\text{P\&T}}^{(2)}(C_S^{(2)}) \rangle = iC_S^{(2)} \frac{G_F}{\sqrt{2}} (\bar{\psi}_n \gamma^5 \psi_n) (\bar{\psi}_e \psi_e), \quad (31b)$$

where $G_F = 2.223 \times 10^{-14}$ a.u. is the Fermi constant, γ_5 is taken to be

$$\begin{pmatrix} 0 & I \\ I & 0 \end{pmatrix}$$

and $C_S^{(1,2)}$ represent the strengths of the interactions. In the limit of low electron momentum it can be shown [34] that $H_{\text{P\&T}}^{(1)}$ is proportional to the electron spin, resulting in a cancellation of this coupling in TIF just as in the case of the electron EDM. In order to estimate its effect in TIF one has to consider once again the third-order perturbation involving the hyperfine interaction. In our standard form, $H_{\text{P\&T}}(C_S^{(1)}) = -hd_{C_S^{(1)}} \sigma \cdot \hat{\lambda}$, the result found by Flambaum and Khriplovich [9] is

$$\frac{d_{C_S^{(1)}}}{C_S^{(1)}} = 22 \text{ Hz}. \quad (32)$$

When combined with our experimental result this gives the limit

$$C_S^{(1)} = (-6 \pm 10) \times 10^{-6}. \quad (33)$$

A similar perturbation expansion can be made for $C_S^{(2)}$ [9], however, this interaction is suppressed by an additional factor of order electron mass over nuclear mass, so the corresponding limit on $C_S^{(2)}$ is several orders of magnitude weaker than that on $C_S^{(1)}$.

For the tensor-pseudotensor interaction, the Hamiltonian is

$$H_{\text{P\&T}}(C_T) = iC_T \frac{G_F}{\sqrt{2}} (\bar{\psi}_n \sigma^{\mu\nu} \psi_n) (\bar{\psi}_e \gamma^5 \sigma_{\mu\nu} \psi_e). \quad (34)$$

In this case there is only one Hamiltonian because the interaction turns out to be the same whether the γ_5 is in the nuclear or the electronic current. As usual, it can be written [10] in the effective form $H_{\text{P\&T}}(C_T) = -hd_{C_T} \sigma \cdot \hat{\lambda}$. According to the calculation by Coveney and Sandars [29,35], the coupling constant has the value

$$\frac{d_{C_T}}{C_T} = 851 \text{ Hz}. \quad (35)$$

In combination with our experimental result this yields the limit

$$C_T = (-1.5 \pm 2.6) \times 10^{-7}. \quad (36)$$

One can also imagine P&T-odd interactions between one nucleon and another. Flambaum, Khriplovich, and Sushkov [36] have estimated the Schiff moment Q_η that would result from such internal forces if they were present in the TI nucleus. For a scalar-pseudoscalar interaction they find

$$Q_\eta = (1.2\eta_{p-p} - 1.4\eta_{p-n}) \times 10^{-8} e \text{ fm}^3, \quad (37)$$

where η measures the proton-proton ($p-p$) or proton-neutron ($p-n$) coupling in units of the Fermi constant. In

TABLE VI. Sensitivity of TIF to various P&T-violating effects. There are many different mechanisms that may give rise to P&T-violation in TIF. Characteristic strengths of such mechanisms can be related to the coupling constant d of the effective Hamiltonian. Here we list the conversion factors from the measured value of d to the strengths of possible P&T violations in TIF.

Source of P&T violation	Sensitivity of TIF
EDM of $J=1, F=2$ state of TIF	$\frac{d}{d_{\text{TIF}}} = 7.60 \times 10^{18} \frac{\text{Hz}}{e \text{ cm}}$
Proton EDM	$\frac{d}{d_p} = 3.52 \times 10^{18} \frac{\text{Hz}}{e \text{ cm}}$
Schiff moment	$\frac{d}{Q} = -5.67 \times 10^5 \frac{\text{Hz}}{e \text{ fm}^3}$
Electron EDM	$\frac{d}{d_e} = 6.24 \times 10^{20} \frac{\text{Hz}}{e \text{ cm}}$
Weak scalar-pseudoscalar $e-N$ interaction	$\frac{d_{C_S^{(1)}}}{C_S^{(1)}} = 22 \text{ Hz}$
Weak-tensor $e-N$ interaction	$\frac{d_{C_T}}{C_T} = 851 \text{ Hz}$
Weak scalar-pseudoscalar $N-N$ interaction	$\frac{d_\eta}{1.2\eta_{p-p} - 1.4\eta_{p-n}} = -5.67 \times 10^{-3} \text{ Hz}$

TABLE VII. Limits on T-violation parameters from recent atomic experiments. The TIF and TI experiments both used the beam resonance technique, whereas the Hg and Cs experiments were done on optically pumped atoms in cells.

	Hg (Ref. [28])	TIF	Cs (Ref. [37])	TI (Ref. [26])
EDM of system (e cm)	$(0.7 \pm 1.5) \times 10^{-26}$	$(-1.7 \pm 2.9) \times 10^{-23}$	$(-1.8 \pm 6.9) \times 10^{-24}$	$(1.6 \pm 5) \times 10^{-24}$
Schiff moment Q (e fm ³)	$(-2 \pm 4) \times 10^{-10}$	$(2 \pm 4) \times 10^{-10}$		
Proton EDM d_p (e cm)		$(-4 \pm 6) \times 10^{-23}$		
Electron EDM d_e (e cm)	$(-5 \pm 11) \times 10^{-25}$	$(-2 \pm 4) \times 10^{-25}$	$(-2 \pm 6) \times 10^{-26}$	$(-3 \pm 8) \times 10^{-27}$
$C_S^{(1)}$	$(10 \pm 22) \times 10^{-6}$	$(-6 \pm 10) \times 10^{-6}$	$(3 \pm 10) \times 10^{-6}$	$(2 \pm 7) \times 10^{-7}$
C_T	$(-1 \pm 3) \times 10^{-7}$	$(-2 \pm 3) \times 10^{-7}$		

conjunction with our measurement this gives the limit

$$1.2\eta_{p-p} - 1.4\eta_{p-n} = (-2.3 \pm 3.9) \times 10^{-2}. \quad (38)$$

All these relations between the measured P&T-odd coupling constant d and the more basic quantities are summarized in Table VI.

G. P-even, T-odd couplings

Experiments of this kind are normally viewed as a search for P&T-odd fundamental interactions. Recently, however, Khriplovich [11] has pointed out that the P&T-odd effective Hamiltonian $-d\sigma \cdot \hat{\lambda}$ can be produced by a T-odd, P-even interaction as a result of P-odd electroweak radiative corrections. He finds that some of those one-loop corrections are smaller than the leading P-even term only by a factor of order α/π . On this basis he is able to use our result in TIF to obtain new limits on P-even, T-odd interactions. He finds, for example, that the P-even, T-odd quark-quark interactions are less than 30 times the weak interaction strength. In addition, he is able to deduce limits at the 10^{-3} level on the T-odd, P-even β -decay constants. Our measurement, the other atomic EDM experiments and the neutron measurements are all of comparable sensitivity in this respect and together they furnish the best limits on such interactions.

VI. CONCLUSION

The significance of our measurement can be summarized as follows. Our result provides the best limit on the

proton EDM d_p and also places stringent limits on the e - N tensor coupling C_T , the nuclear Schiff moment Q , and T-odd N - N interactions. Limits derived from this experiment on the electron EDM d_e and on the scalar e - N interaction $C_S^{(1)}$ are strong, but not as good as those found using paramagnetic atoms. The current situation is summarized in Table VII where we show the limits implied by our result, together with those obtained from other experiments.

Looking to the future, we believe that the TIF beam apparatus at Yale, which has achieved improvements by a factor of 50 over the past few years, can still make an order of magnitude improvement over the present work. Some of the remaining systematics should, however, be understood in more detail. In the long run it may be necessary to find ways of slowing and trapping TIF molecules in order to reduce the large linewidth (100 Hz) of the resonance.

ACKNOWLEDGMENTS

The contributions made by G. L. Greene, T. Vold, and D. Schropp, Jr. during earlier stages of this project are greatly appreciated. We are also indebted to Professor J. Fenn for his advice in developing our jet source and to M. Krasberg for his work on the project. Much of the expertise required to construct the machine was provided by R. Broughton and by members of the Gibbs Instrumentation Shop led by G. Vogel. This work was supported by the National Science Foundation.

- [1] T. D. Lee and C. N. Yang, Phys. Rev. **104**, 254 (1956).
- [2] C. S. Wu, E. Ambler, R. W. Hayward, D. D. Hoppes, and R. P. Hudson, Phys. Rev. **105**, 1413 (1957).
- [3] J. H. Christenson, J. W. Cronin, V. L. Fitch, and R. Turlay, Phys. Rev. Lett. **13**, 138 (1964).
- [4] E. A. Hinds, in *Atomic Physics 11*, edited by S. Haroche, J. C. Gay, and G. Grynberg (World Scientific, Singapore, 1989), p. 151.
- [5] L. I. Schiff, Phys. Rev. **132**, 2194 (1963).
- [6] P.G.H. Sandars, Phys. Rev. Lett. **19**, 1396 (1967).
- [7] E. A. Hinds and P.G.H. Sandars, Phys. Rev. A **21**, 471 (1980).
- [8] P. V. Coveney and P.G.H. Sandars, J. Phys. B **16**, 3727 (1983).
- [9] V. V. Flambaum and I. B. Khriplovich, Zh. Eksp. Teor. Fiz. **89**, 1505 (1985) [Sov. Phys.—JETP **62**, 872 (1985)].
- [10] E. A. Hinds, C. E. Loving, and P.G.H. Sandars, Phys. Lett. **62B**, 97 (1976).
- [11] I. B. Khriplovich (unpublished).
- [12] G. E. Harrison, P.G.H. Sandars, and S. J. Wright, Phys. Rev. Lett. **22**, 1263 (1969).
- [13] E. A. Hinds and P.G.H. Sandars, Phys. Rev. A **21**, 480 (1980).
- [14] D. A. Wilkening, N. F. Ramsey, and D. J. Larson, Phys.

- Rev. A **29**, 425 (1984).
- [15] D. R. Schropp, Jr., D. Cho, T. Vold, and E. A. Hinds, Phys. Rev. Lett. **59**, 991 (1987).
- [16] D. Cho, K. Sangster, and E. A. Hinds, Phys. Rev. Lett. **63**, 2559 (1989).
- [17] D. R. Schropp, Jr., Ph.D. thesis, Yale University, 1988 (unpublished).
- [18] E. F. Greene, Rev. Sci. Instrum. **32**, 860 (1961).
- [19] P. Kusch and V. W. Hughes in *Handbuch der Physik*, Vol. 37/1, edited by S. Flügge (Springer-Verlag, Berlin, 1959), p. 138.
- [20] N. F. Ramsey, *Molecular Beams* (Oxford University Press, London, 1956).
- [21] N. F. Ramsey and H. B. Silsbee, Phys. Rev. **84**, 506 (1951).
- [22] G. E. Harrison, M. A. Player, and P.G.H. Sandars, J. Phys. E **4**, 750 (1971).
- [23] W. B. Dress, P. D. Miller, J. M. Pendlebury, P. Perrin, and N. F. Ramsey, Phys. Rev. D **15**, 9 (1977).
- [24] J. P. Carrico, E. Lipworth, P.G.H. Sandars, T. S. Stein, and M. C. Wiesskopf, Phys. Rev. **174**, 125 (1968).
- [25] M. A. Player and P.G.H. Sandars, J. Phys. B **3**, 1620 (1970).
- [26] K. Abdullah, C. Carlberg, E. D. Commins, H. Gould, and S. Ross, Phys. Rev. Lett. **65**, 2347 (1990).
- [27] S. Millman, Phys. Rev. **55**, 628 (1939).
- [28] S. K. Lamoreaux, J. P. Jacobs, B. R. Heckel, F. J. Raab, and N. Fortson, Phys. Rev. Lett. **59**, 2275 (1987).
- [29] P. V. Coveney, BA thesis, Lincoln College, Oxford, 1981.
- [30] The value $d^M/d_p = 4.1 \times 10^{-7}$ a.u. given on p. 3737 of Ref. [8] is a misprint. It should read $d^M/d_p = 6.22 \times 10^{-7}$ a.u. as in Ref. [29].
- [31] O. P. Sushkov, V. V. Flambaum, and I. B. Khriplovich, Zh. Eksp. Teor. Fiz. **87**, 1521 (1984) [Sov. Phys.—JETP **60**, 873 (1984)].
- [32] E. E. Salpeter, Phys. Rev. **112**, 1642, (1958).
- [33] E. D. Commins and P. H. Bucksbaum, *Weak Interactions of Leptons and Quarks* (Cambridge University Press, New York, 1983).
- [34] C. Bouchiat, Phys. Lett. **57B**, 284 (1975).
- [35] The value $d_T/C_T = -5.08$ a.u. given on p. 3737 of Ref. [8] is a mistake. It should read $d_T/C_T = -5.82$ a.u. as given in Ref. [29]. The value we quote here has opposite sign to account for a different definition of γ_5 . It has also been corrected for the slightly different value of G_F that Coveney and Sandars used.
- [36] V. V. Flambaum, I. B. Khriplovich, and O. P. Sushkov, Nucl. Phys. A **449**, 750 (1986).
- [37] S. A. Murthy, D. Krause, Jr., Z. L. Li, and L. R. Hunter, Phys. Rev. Lett. **63**, 965 (1989).